

## RESEARCH ARTICLE

10.1002/2015JC011119

## Salt precipitation in sea ice and its effect on albedo, with application to Snowball Earth

Regina C. Carns<sup>1,2</sup>, Richard E. Brandt<sup>3</sup>, and Stephen G. Warren<sup>1,2</sup>

## Key Points:

- Albedo of cold subeutectic natural sea ice in McMurdo Sound is measured
- Sea ice albedo increases at temperatures below  $-23^{\circ}\text{C}$
- Brine in sea ice supercools before sodium chloride precipitates as hydrohalite

## Correspondence to:

R. C. Carns,  
rcarns@uw.edu

## Citation:

Carns, R. C., R. E. Brandt, and S. G. Warren (2015), Salt precipitation in sea ice and its effect on albedo, with application to Snowball Earth, *J. Geophys. Res. Oceans*, 120, 7400–7412, doi:10.1002/2015JC011119.

Received 22 JUL 2015

Accepted 7 OCT 2015

Accepted article online 11 OCT 2015

Published online 18 NOV 2015

<sup>1</sup>Department of Earth and Space Sciences, University of Washington, Seattle, Washington, USA, <sup>2</sup>Astrobiology Program, University of Washington, Seattle, Washington, USA, <sup>3</sup>Atmospheric Sciences Research Center, University at Albany - State University of New York, Wilmington, New York, USA

**Abstract** During the initial freezing of the tropical ocean on Snowball Earth, the first ice to form would be sea ice, which contains salt within inclusions of liquid brine. At temperatures below  $-23^{\circ}\text{C}$ , significant amounts of the salt begin to crystallize, with the most abundant salt being hydrohalite ( $\text{NaCl}\cdot 2\text{H}_2\text{O}$ ). These crystals scatter light, increasing the ice albedo. In this paper, we present field measurements of the albedo of cold sea ice and laboratory measurements of hydrohalite precipitation. Precipitation of salt within brine inclusions was observed on windswept bare ice of McMurdo Sound at the coast of Antarctica ( $78^{\circ}\text{S}$ ) in early austral spring. Salinity and temperature were measured in ice cores. Spectral albedo was measured on several occasions during September and October. The albedo showed a gradual increase with decreasing temperature, consistent with salt precipitation. Laboratory examination of thin sections from the ice cores showed that the precipitation process exhibits hysteresis, with hydrohalite precipitating over a range of temperatures between  $-28^{\circ}\text{C}$  and  $-35^{\circ}\text{C}$  but dissolving at about  $-23^{\circ}\text{C}$ . The causes of the hysteresis were investigated in experiments on laboratory-grown sea ice with different solute mixtures. All mixtures showed hysteresis, suggesting that it may be an inherent property of hydrohalite precipitation within brine inclusions rather than being due to biological macromolecules or interactions between various salts in seawater.

## 1. Introduction

As new sea ice grows, inclusions of seawater become trapped in the thickening ice. These brine inclusions have typical diameters 10–200  $\mu\text{m}$ , and can have average number densities as high as 20  $\text{mm}^{-3}$  [Weeks and Ackley, 1982; Perovich and Gow, 1991, 1996; Light et al., 2003]. Consequently, the salinity of young ice is 12–20 parts per thousand (‰) by mass when growing from seawater of normal salinity (32–35‰). With further cooling during winter, some of the water in the brine inclusions freezes; the increase in pressure causes cracks to form, and some of the brine is expelled, reducing the bulk salinity. The surface salinity of first-year sea ice can vary between 8 and 16‰ [Cox and Weeks, 1988].

As the upper layers of the ice cool, water in a brine inclusion freezes to the walls of the inclusion, so that the salinity of the remaining liquid adjusts to that required for phase equilibrium at the lower temperature. As the concentration of ions increases, salts precipitate out of solution, including ikaite ( $\text{CaCO}_3\cdot 6\text{H}_2\text{O}$ ) near the freezing point of seawater [Hu et al., 2014], and mirabilite ( $\text{Na}_2\text{SO}_4\cdot 10\text{H}_2\text{O}$ ) around  $-8^{\circ}\text{C}$  [Marion et al., 1999]. The major salt in seawater is NaCl. For a binary mixture of NaCl and  $\text{H}_2\text{O}$  in equilibrium, the NaCl precipitates as the dihydrate  $\text{NaCl}\cdot 2\text{H}_2\text{O}$  (“hydrohalite”) at the eutectic temperature of  $-21.1^{\circ}\text{C}$ . When accompanied by the mixture of salts present in natural seawater, hydrohalite begins to precipitate at  $-22.9^{\circ}\text{C}$  [Spencer et al., 1990; Wettlaufer, 1998]. For brevity, in this paper, we will use the term “subeutectic” to refer to natural sea ice colder than  $-22.9^{\circ}\text{C}$ .

### 1.1. Hydrohalite Occurrence and Influence on Snowball Earth

The precipitated salt crystals can scatter sunlight, but only if sunlight is available. On the modern Earth, temperatures low enough to cause salt precipitation occur only during winter on the polar oceans, when there is little sunlight and when the ice is usually hidden beneath a layer of snow. The increase in albedo caused by salt precipitation in sea ice therefore is not significant for climate on the modern Earth, but it could have been important at times in the distant past. In particular, the “Snowball Earth” events of the Neoproterozoic (600–800 million years ago) [Hoffman and Schrag, 2002] may have been characterized by a frozen ocean

with tropical surface temperatures below  $-30^{\circ}\text{C}$  in all months [Pollard and Kasting, 2004, Figure 7; Pierrehumbert, 2005, Figure 2].

In some oceanic regions of Snowball Earth, the ice surface would have been mostly free of snow. On the modern Earth, evaporation exceeds precipitation on the subtropical oceans,  $\sim 20^{\circ}$ – $30^{\circ}$  latitude. On the Snowball planet, by contrast, the Hadley-cell circulation is altered so that the zone of net sublimation would instead be centered at the equator [Pierrehumbert et al., 2011], but would encompass large areas of the tropical ocean [Pollard and Kasting, 2004; Pierrehumbert et al., 2011].

In Snowball Earth scenarios, ice extends to low latitudes where it is exposed to intense sunlight, so small changes in surface albedo can have significant consequences in climate models. For example, Pierrehumbert et al. [2011] showed that a change of ice albedo from 0.55 to 0.65 means that a factor-of-10 increase in the mixing ratio of atmospheric  $\text{CO}_2$  is required to end the snowball state. Abbot et al. [2011] found that a narrow belt of open water could persist along the equator if the sea-ice albedo was 0.45 but not if it was  $\geq 0.55$ . Yang et al. [2012] found that a change of prescribed albedo from 0.55 to 0.58 had large effects on the speed of snowball initiation and on the eventual fraction of the ocean covered by sea ice in equilibrium. To improve the realism of these models, we are working to determine accurate albedos for the variety of ice types that might have existed on the snowball ocean.

### 1.2. Ice Types on Snowball Earth and Modern Analogues

In zones of net sublimation, the ocean surface would have exhibited a sequence of four ice types with different albedos. Newly formed sea ice without salt precipitation, ice type (1), would resemble the rapidly growing new sea ice found in polar winters today. Later, as the interior ice temperatures dropped below the temperature of initial precipitation, salt would crystallize in brine inclusions, forming ice type (2): cold “subeutectic” sea ice. A salt crust would develop as a “lag deposit” after significant loss of ice to sublimation; cold ice with a salt crust constitutes ice type (3). Finally, the ice cover on the midlatitude and polar oceans, built up from above by snowfall and from below by freezing of seawater, would be expected to reach thicknesses of several hundred meters. This thickness is sufficient to permit flow as “sea glaciers,” like modern ice shelves but not dependent on continental glaciation for their existence [Goodman and Pierrehumbert, 2003; Goodman, 2006]. The sea glaciers flowing toward the equator (and sublimating) would likely displace the sea ice, but in some models the sea ice persists [Pollard and Kasting, 2005, 2006; Warren and Brandt, 2006]. The sublimating sea-glacier surface would be freshwater ice: ice type (4). Its albedo would be determined by its bubble content.

The albedo of ice type (1) has been measured at the coast of Antarctica at a temperature of  $-5^{\circ}\text{C}$  [Brandt et al., 2005, Figure 1; Warren et al., 2002, Figure 8]. Ice type (4), the ice of sublimating sea glaciers, has been measured in the blue-ice regions of the Transantarctic Mountains [Dadic et al., 2013]. Ice type (3), the salt crust, apparently does not occur on the modern Earth, because the atmospheric conditions favoring ablation by sublimation do not persist long enough before the springtime warming. Therefore, to investigate that surface type, we are sublimating artificial sea ice in our freezer laboratory [Light et al., 2015]. Ice type (2), the subeutectic sea ice, is the topic of this paper.

Sea ice that formed during the rapid freezing phase of a snowball event would probably not experience surface melting, so it would not experience the annual flushing events that purge salt from the upper ice layers on the modern Earth. Instead, salt would remain within brine inclusions, precipitating at low temperatures and increasing the albedo of the ice. Our measurements of the albedo of subeutectic sea ice in nature, reported in this paper, were motivated by the dramatic result of a laboratory experiment reported by Perovich and Grenfell [1981]. In that experiment, laboratory-grown sea ice, containing NaCl as its only salt, was illuminated by a broad-spectrum light. At an ambient temperature of  $-37^{\circ}\text{C}$ , the spectral albedo was extremely high; as the temperature was raised to  $-22^{\circ}\text{C}$ , just above the eutectic temperature of  $-22.9^{\circ}\text{C}$ , the albedo dropped dramatically (Figure 1).

Light et al. [2003, 2004] also investigated the precipitation of hydrohalite in first-year sea ice and its effects on the optical properties of the ice. They measured transmittance instead of albedo, but their results also showed a change with salt precipitation. They found that the transmittance of natural ice in the laboratory dropped slightly during initial cooling to  $-20^{\circ}\text{C}$ , above the precipitation temperature of hydrohalite, and then dropped dramatically when the ice was cooled to  $-25^{\circ}\text{C}$  (Figure 2). To examine hydrohalite

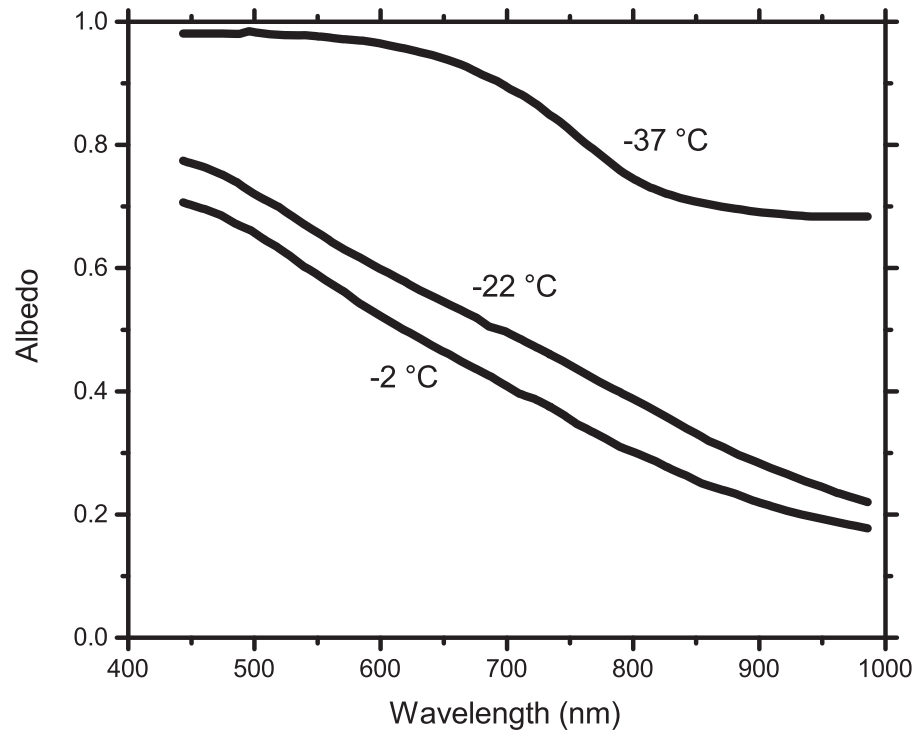


**Figure 1.** Spectral albedos of artificial salt-ice (containing NaCl as the only salt), measured in a freezer laboratory as the temperature was increasing from  $-37^{\circ}\text{C}$ . The albedo curves are labeled with laboratory air temperatures at the time they were measured. Redrawn from *Perovich and Grenfell [1981]*, with modifications.

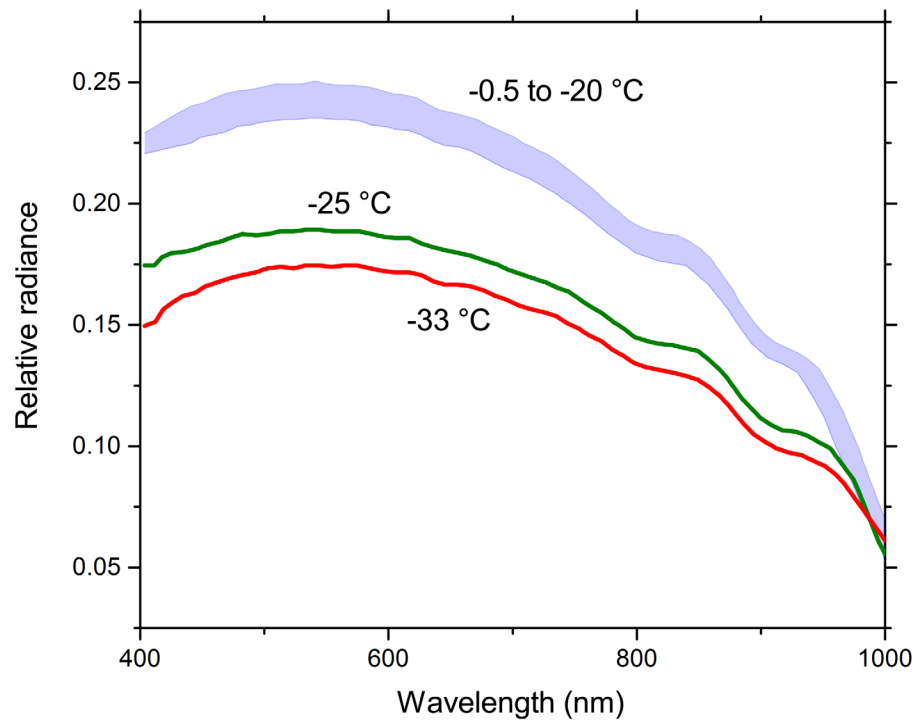


**Figure 2.** Temperature-dependent changes in the spectral radiance of transmitted light, normalized by the incident irradiance. At  $-25^{\circ}\text{C}$  and  $-33^{\circ}\text{C}$ , highly scattering hydrohalite crystals block a significant fraction of the light. Redrawn from *Light et al. [2004]*, with modifications.



**Figure 3.** ASD radiometer measuring spectral albedo of sea ice in McMurdo Sound. Note cleared area, from which the 3 mm crust of salty snow has been removed; 78°S, September 2009.

precipitation (and its effect on albedo) in nature, the ice must satisfy four criteria: it should be first-year ice (i.e., has not experienced summer drainage of brine), snow-free, colder than  $-23^{\circ}\text{C}$ , and exposed to adequate sunlight or twilight for visible and near-infrared radiation measurements. These criteria are satisfied by shorefast sea ice in many places along the coast of Antarctica during late winter and early spring, at locations where the snow is blown away by wind [Purdie *et al.*, 2006]. Ice that has survived a summer melt season (multiyear ice) has become largely desalinated by flushing of meltwater [Untersteiner, 1968], so salt precipitation will be most readily apparent only in first-year ice.

## 2. Field Measurements

We drove about 100 km of reconnaissance on the landfast sea ice of McMurdo Sound between McMurdo Station and Cape Royds; the best site for snow-free first-year ice was identified on the west side of Tent Island, one of the Delbridge Islands. Figure 3 is a photograph of our principal site at  $77.68^{\circ}\text{S}$ ,  $166.35^{\circ}\text{E}$ . Ice temperatures at the surface and at 10 cm depth were measured using thermistors embedded in the ice and logged at 1 min intervals using a Campbell CR10X data logger. The difference between the surface and 10 cm depth varied from 0 to 3 K, with periods of gradual cooling and rapid warming. The measurements taken on 22, 23, and 26 September were taken during a several-day period of cooling, during which the ice temperature decreased steadily with only small diurnal changes, and never increased above  $-23^{\circ}\text{C}$  after falling below it. The 5 October measurement was taken at the peak of a 2 day warming period, during which the surface temperature increased from  $-24^{\circ}\text{C}$  to  $-18^{\circ}\text{C}$ .

Several ice cores were extracted to examine temperature and salinity profiles and ice microstructure, using a manually operated ice-coring drill which cut cores with diameter 10 cm. Some of these ice cores were 1 m long; others included only what we considered to be the portion of the ice relevant to albedo, approximately the upper 30 cm.

The ice salinity (Figure 4) was 10‰ at the surface, decreasing to 6‰ at 30 cm, and then nearly constant at 5–7‰ down to 90 cm. A 3 mm surface crust of higher salinity (about 18‰) was often present. A research

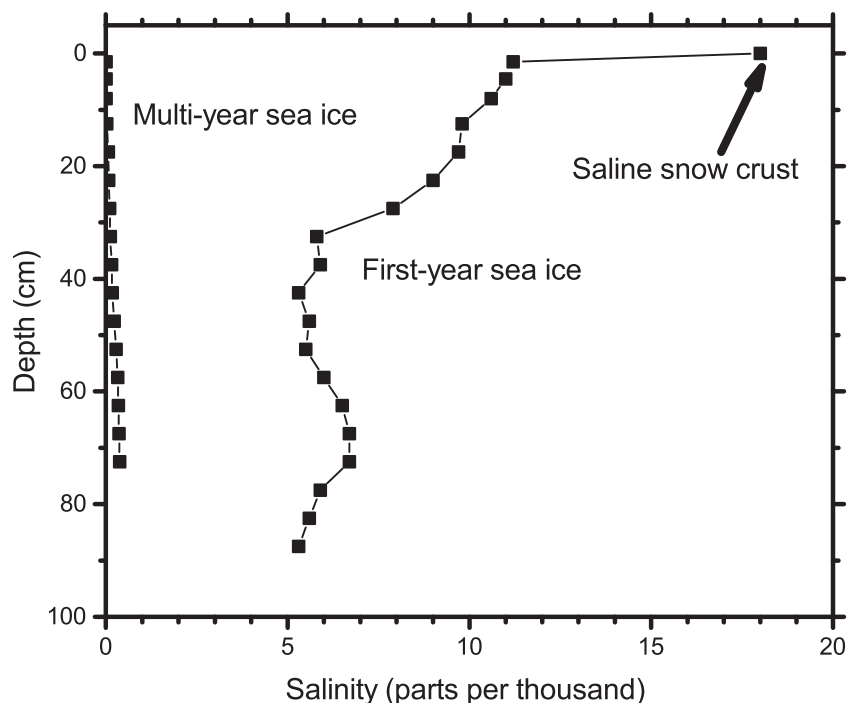


**Figure 4.** Salinity of ice in McMurdo Sound as a function of depth, measured in sections of 1 m cores. The core of first-year ice was taken from the site for albedo measurement; the core of multiyear ice (MYI) was taken near the shore of Ross Island, 12 km farther south. The very low salinity of the MYI is the result of brine drainage during summer. The salinity at the top of the MYI is 7 ppm.

group of the New Zealand Antarctic Programme (NZAP), who had monitored the sea ice in McMurdo Sound throughout that winter, had observed this crust to form during the early stages of freezing in autumn as a result of metamorphism of “frost flowers” [Perovich and Richter-Menge, 1994; Rankin *et al.*, 2002; Style and Worster, 2009]. However, the crust reformed later after we removed it from the surface, suggesting that it could also (or instead) be windblown snow which stuck to a thin film of brine seeping from the top of the ice (H. Eicken, personal communication, 2009).

Ice temperatures at the study site varied with time and depth, crossing the threshold for hydrohalite precipitation. On one occasion, the surface brightening was visible by eye as the ice cooled in late afternoon and salt crystallization occurred in patches then spread throughout the area.

We measured spectral albedo on seven occasions, both for the intact ice and after removal of the snow-like surface crust; both types may be relevant for Snowball Earth. Spectral albedo measurements are most accurate under diffuse illumination, so we favored measurements made under overcast sky or in the shadow of the adjacent islands. The albedo was measured using a portable scanning spectroradiometer manufactured by Analytical Spectral Devices (ASD) [Kindel *et al.*, 2001]. The instrument employs three separate grating spectrometers that simultaneously measure radiance across three wavelength regions covering 350–2500 nm, with spectral resolution 3–10 nm, and can average 100 scans in 10 s. It is designed specifically to cover the solar spectrum, and has order-blocking and cutoff filters to ensure uncontaminated spectra.

The ASD radiometer and its computer were both battery powered and housed in separate insulated boxes. At ambient temperatures of  $-20$  to  $-35^{\circ}\text{C}$ , the electronics were kept warm by self-heating supplemented by battery-powered heaters. For albedo measurements, a Spectralon diffuser-plate receptor was mounted on a rod suspended 0.7 m above the ice, supported at one end by a tripod resting on the ice (Figure 3). The light is carried by a fiber-optic guide to the radiometer.

### 2.1. Results of Field Measurements

As the temperature drops below the initial precipitation point of hydrohalite, the albedo of bare sea ice in McMurdo Sound increases. Figure 5 shows spectral albedos of the bare sea ice (after removal of the snow-like surface crust) in McMurdo Sound for four ice temperatures. As expected, the colder ice does exhibit

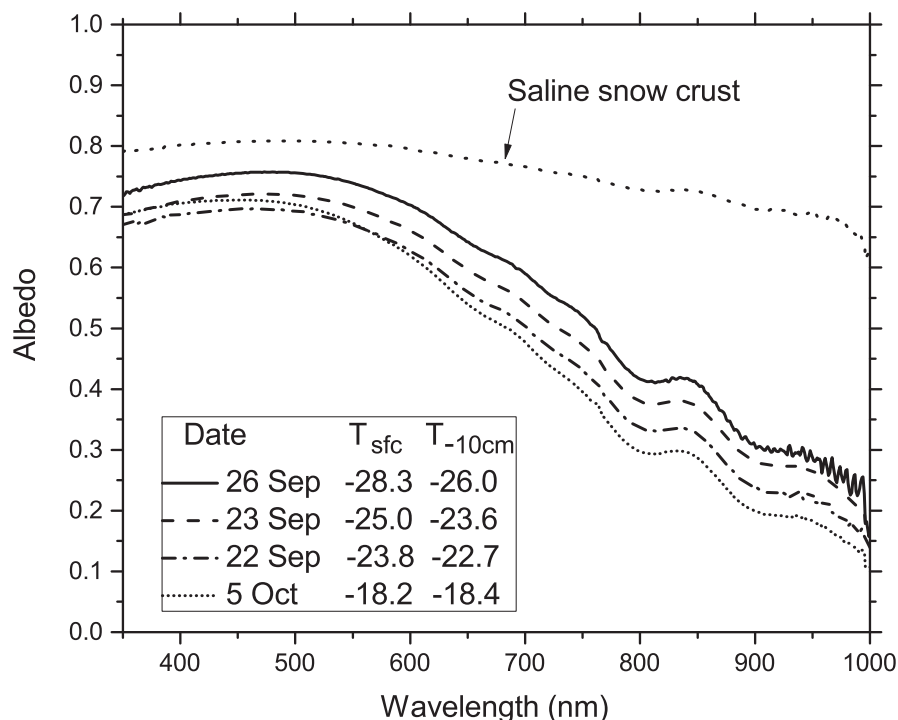


**Figure 5.** Spectral albedos of sea ice in McMurdo Sound during September and October of 2009. Except for the top curve, all measurements were of ice whose surface crust of salty snow had been scraped off. Legend shows date of measurement, surface temperature at time of measurement, and temperature at 10 cm depth at time of measurement for each curve.

higher albedo. However, the apparent dramatic jump in albedo for subeutectic ice seen in the laboratory experiments on artificial NaCl-ice [Perovich and Grenfell, 1981] does not appear in our McMurdo albedos. The albedos are also lower than expected from the results of Perovich and Grenfell [1981], who found visible albedo  $>0.9$  for subeutectic ice. In their case, the ice surface temperature was  $-32^{\circ}\text{C}$ , colder than any of our profiles, although its temperature at 10 cm below the surface was  $-20^{\circ}\text{C}$  [Perovich, 1979, p. 86]. Their ice was also grown at a constant  $-37^{\circ}\text{C}$ , while average air temperatures in McMurdo Sound during the period of initial ice formation were closer to  $-20^{\circ}\text{C}$ . Lower temperatures at the time of ice formation lead to faster ice growth, which in turn leads to higher-salinity ice and to higher albedos at a given temperature [Perovich and Grenfell, 1981] so this may also have contributed to the higher albedo of the laboratory ice.

The spectral albedos are integrated over three broad wavelength-bands, using an incident solar spectrum obtained from an atmospheric radiation model. Two solar spectra are used, one for clear sky and one for cloudy sky; they are similar to solar spectra shown in Brandt and Warren [1993, Figure 1]. These broadband albedos are plotted versus ice surface temperature in Figure 6, showing the gradual slight decrease of albedo as the temperature rose from  $-29^{\circ}\text{C}$  to  $-18^{\circ}\text{C}$ . Even at the lowest temperature, the broadband albedos are close to the value 0.49 measured for bare sea ice near Davis Station at  $-5^{\circ}\text{C}$ , well above the temperature where significant salt precipitation would be expected [Brandt et al., 2005, Figure 1]. Our laboratory measurements indicate that precipitation continues well below  $-28^{\circ}\text{C}$ , so lower temperatures would likely result in higher albedos.

### 3. Laboratory Measurements

Our laboratory experiments were motivated by our observations of sea ice in the field, which showed a gradual increase in albedo, rather than the discontinuous jump we had been led to expect by laboratory observations. We hypothesized that the difference between our results and those of Perovich and Grenfell could be due to the natural ice undergoing supersaturation, with sodium chloride in some brine inclusions resisting precipitation. The results of Perovich and Grenfell do not exclude this possibility, since their albedos were taken during warming rather than during cooling. Supersaturation of solutions containing sodium chloride

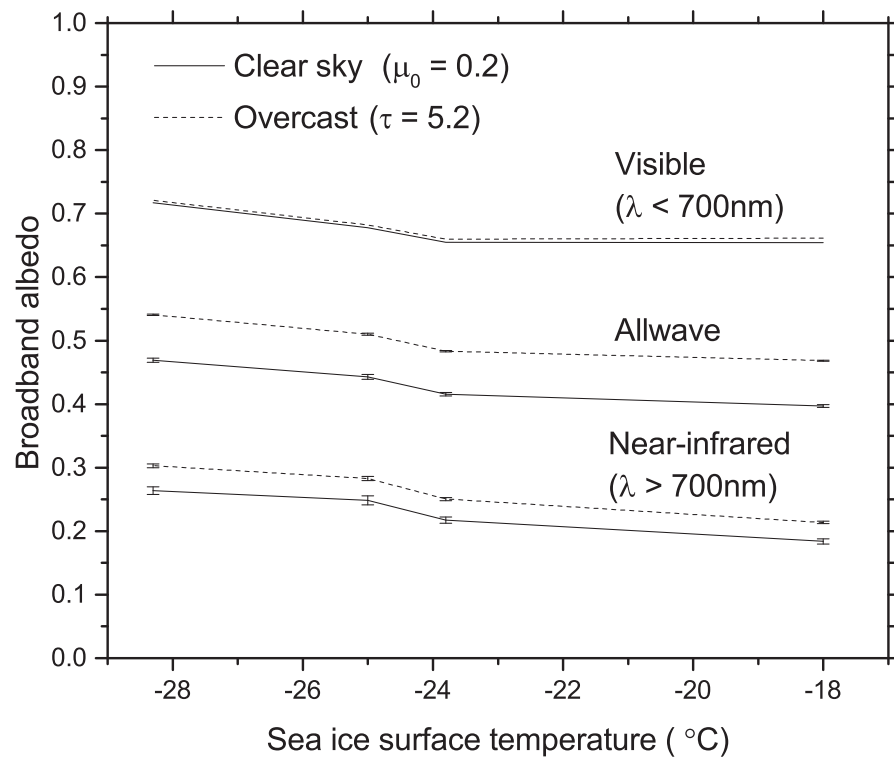


**Figure 6.** Broadband albedo as a function of temperature for three wavelength bands. To compute broadband albedo  $\bar{\alpha}$ , the spectral albedos  $\alpha(\lambda)$  of Figure 5 are weighted by the incident solar spectra  $F(\lambda)$  from an atmospheric radiation model [Wiscombe *et al.*, 1984]:

$$\bar{\alpha} = \frac{\int \alpha(\lambda) F(\lambda) d\lambda}{\int F(\lambda) d\lambda}$$

The limits of integration for the “allwave” band are 290 and 3000 nm. For the wavelengths not measured, albedos for  $\lambda < 350$  nm were set to that of 350 nm; albedos for  $\lambda > 1500$  nm were set to that of 1500 nm, as discussed by Brandt *et al.* [2005].

Two atmospheric conditions are considered: clear sky at zenith-angle cosine  $\mu_0 = 0.2$  (solar zenith angle  $78.5^\circ$ ), and overcast cloud of optical thickness  $\tau = 5.2$ , with a base at 1.27 km above the surface (cloud thickness 1.46 km). Atmospheric temperature and humidity profiles are modified from the subarctic winter profile of McClatchey *et al.* [1972], as follows: All temperatures were multiplied by 0.9730 so that the surface temperature is 250 K; water vapor was scaled at each level to preserve the relative humidities of McClatchey *et al.* [1972].

has been previously reported in sea ice [Light *et al.*, 2003; Pringle *et al.*, 2009] as well as in biological contexts [Han and Bischof, 2004]. We therefore initiated laboratory experiments to investigate this possibility.

### 3.1. Temperature Cycling of Natural Sea Ice

We extracted cores of the ice near our measurement site as described in the previous section. The cores were transported from the field at ambient temperatures (generally between  $-30^\circ\text{C}$  and  $-20^\circ\text{C}$ ) and stored in freezers at McMurdo Station ( $-20^\circ\text{C}$ ). We used a bandsaw in a  $-20^\circ\text{C}$  cold room to cut sections of ice  $< 1$  cm in thickness from the cores, cutting along the vertical axis of the core with respect to its original orientation in situ. The sections were taken from the top or near the top of the core, since we were most interested in the brine inclusions at or near the surface where their influence on the ice albedo would be greatest.

Sections were mounted on glass slides and a microtome was used to shave each face, giving the sections optically smooth surfaces and reducing their thickness to a few millimeters. After preliminary imaging at McMurdo Station, the sections were transported at  $-60^\circ\text{C}$  back to the laboratory at the University of Washington, where they were stored at  $-20^\circ\text{C}$ .

Thin sections were prepared for observation under a microscope in our cold-room laboratory by first freezing a temperature probe to the surface of the thin section. Temperature cycling of the ice was achieved by setting the laboratory temperature to either  $-15^\circ\text{C}$  or  $-40^\circ\text{C}$  and allowing it to come to equilibrium at that temperature, generally over a period of 5–7 h of rapid temperature change ( $3\text{--}4^\circ\text{C}$  per hour) followed by 12–24 h of

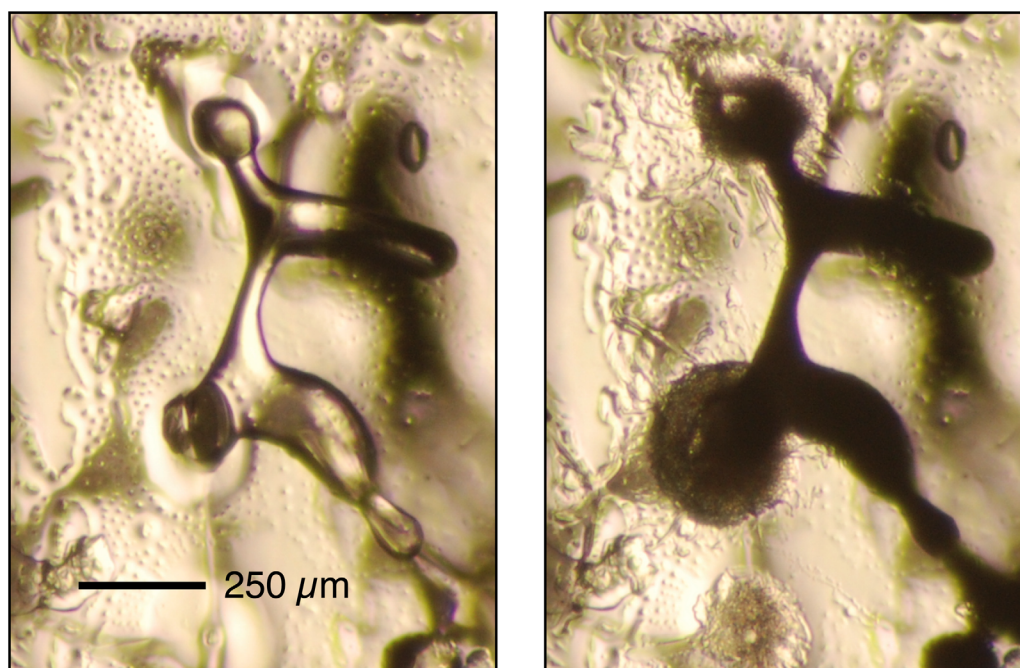


**Figure 7.** A brine pocket in lab-grown ice viewed under a microscope in transmitted light. In the left-hand image, the brine pocket is filled with liquid; in the right-hand image the sodium chloride has crystallized as hydrohalite, filling the pocket with small crystals that block the light. The images were taken 15 min apart at  $-28.7^{\circ}\text{C}$ .

stable temperature (excursions of up to 3 K above the set temperature occurred during defrost cycles). A Nikon D40 DSLR camera attached to the microscope was used to take pictures of the ice at 5 min intervals as the temperature of the cold room changed (Figure 7). Sample temperatures were monitored at 10 s intervals.

The highly scattering nature of hydrohalite crystals makes it easy to detect their presence. A pocket full of clear liquid brine transmits approximately the same amount of light as the ice around it, but after hydrohalite precipitates within the pocket, the small crystals block most of the light coming from below. This property allowed us to use image-analysis software (“ImageJ”) [Abràmoff *et al.*, 2004] to detect how much of the image area had changed in brightness as a proxy for the amount of hydrohalite precipitation. A MATLAB script matched photos to the temperature at the time they were taken. Figure 8 shows the results of this analysis.

The images showed that hydrohalite did not begin to precipitate within brine inclusions until temperatures well below the expected  $-23^{\circ}\text{C}$ , with the first precipitation occurring around  $-28^{\circ}\text{C}$ . The precipitation occurred unevenly; within each individual brine pocket it was rapid and complete, but individual brine inclusions precipitated at different temperatures. Even at  $-38^{\circ}\text{C}$ , some brine inclusions remained completely transparent, likely indicative of a lack of salt precipitation. However, on warming, the crystals dissolved at about  $-23$  to  $-24^{\circ}\text{C}$ , close to the expected temperature.

We hypothesized that precipitation in some brine inclusions may be retarded by the presence of other constituents within certain brine inclusions. Since the presence of other sea salts is known to depress the precipitation point of hydrohalite from  $-21.2^{\circ}\text{C}$  to  $-22.9^{\circ}\text{C}$ , perhaps it might also lead to supersaturation of some brine inclusions. Alternatively, since the sea ice we measured was natural rather than laboratory-grown, it undoubtedly contained microbial life forms. Sea-ice algae and bacteria are known to produce large quantities of mucus-like extracellular polysaccharides (EPS) [Krembs *et al.*, 2011] that may interfere with hydrohalite crystallization. Krembs *et al.* [2011] did show that the EPS influences the structure of brine inclusions and channels, tending to make them more tortuous and interconnected.

### 3.2. Temperature Cycling of Artificial Sea Ice

To investigate these possible reasons for the uneven crystallization, we grew artificial sea ice in the laboratory with three different compositions. The first sample was frozen from an initial solution of water and pure NaCl, as used by Perovich and Grenfell [1981]. The salinity of the solution, approximately half that of

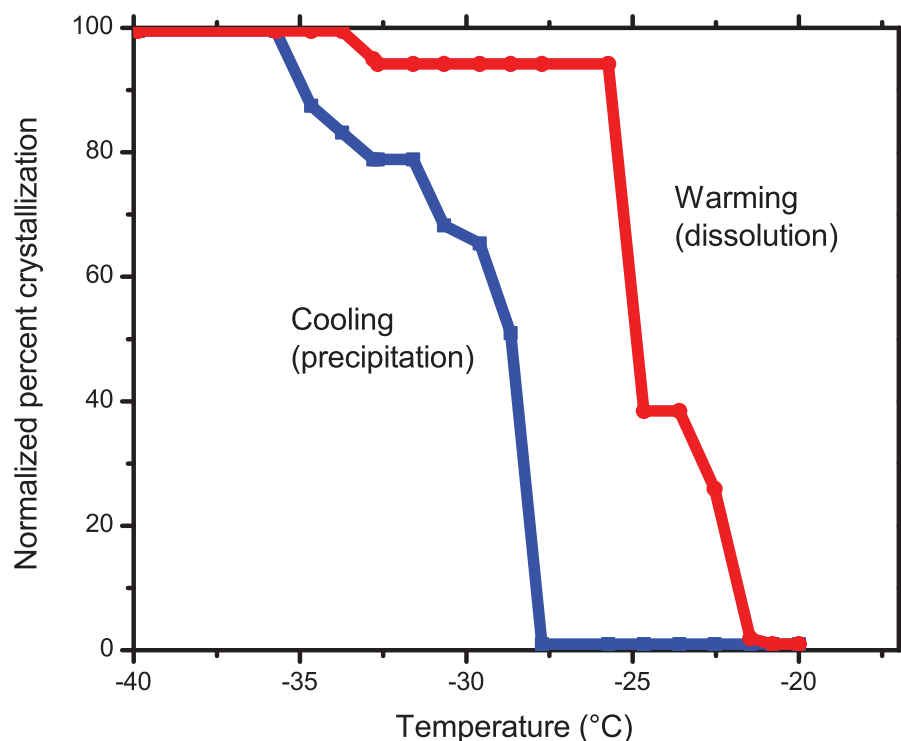


**Figure 8.** Hysteresis during a single temperature cycle of a thin section from an ice core taken in McMurdo Sound. The plot shows the amount of brine pocket area within the microscope's field of view that has crystallized, measured as a percentage of the total area of hydrohalite precipitation at the lowest temperature reached during the experiment.

seawater at 18‰, was chosen because rejection of salt by the freezing ice concentrates the remaining solution, so starting at a lower concentration than seawater allows the middle portion of the sample to freeze from solution with a concentration close to that of seawater. The results in *Perovich and Grenfell* [1981] used ice frozen from a solution of 31.1‰ [Perovich, 1979, p. 49].

The second sample was frozen from an initial solution consisting of artificial seawater made from *Sigma Artificial Sea Salts* at a concentration of 18‰. These salts replicate the ionic composition of seawater but are free from biological material. The third was frozen from an artificial seawater solution to which 1000 mg/L of xanthan gum, a form of EPS, had been added. This concentration was chosen to be several times that found in natural sea ice, where the bulk concentration of EPS can be up to 200 mg/L [Krems et al., 2002]. We hoped that the high concentration would increase the magnitude of any effects EPS might have on the precipitation of hydrohalite, making them easier to observe.

The artificial sea ice was frozen at approximately  $-25^{\circ}\text{C}$  in cylindrical containers with an inner diameter of 10 cm and a depth of 25 cm, constructed from expanded polystyrene foam lined with thin plastic. The foam containers insulated the bottom and sides of the artificial seawater samples, encouraging them to freeze only from the top down, so that the structure of ice crystals and brine inclusions would resemble that of natural sea ice. The samples were allowed to remain at  $-25^{\circ}\text{C}$  for several days to ensure that they froze completely. After freezing, the laboratory-grown samples were processed in the same way as the samples of natural sea ice: sectioned, frozen to glass plates and subjected to temperature cycling in a freezer laboratory.

Figure 9 shows the hysteresis in precipitation and dissolution of brine inclusions within sections taken from lab-grown salty ice. The results suggest that supersaturation of the solutions cannot be attributed to interactions of NaCl with other salts or with polysaccharide material, since all three solutions show precipitation occurring at a temperature approximately 5 K below the temperature of dissolution.

The hydrohalite in the ice containing xanthan gum precipitated at a slightly higher temperature than the ice containing only artificial sea salt, suggesting that the xanthan gum acted to promote precipitation rather

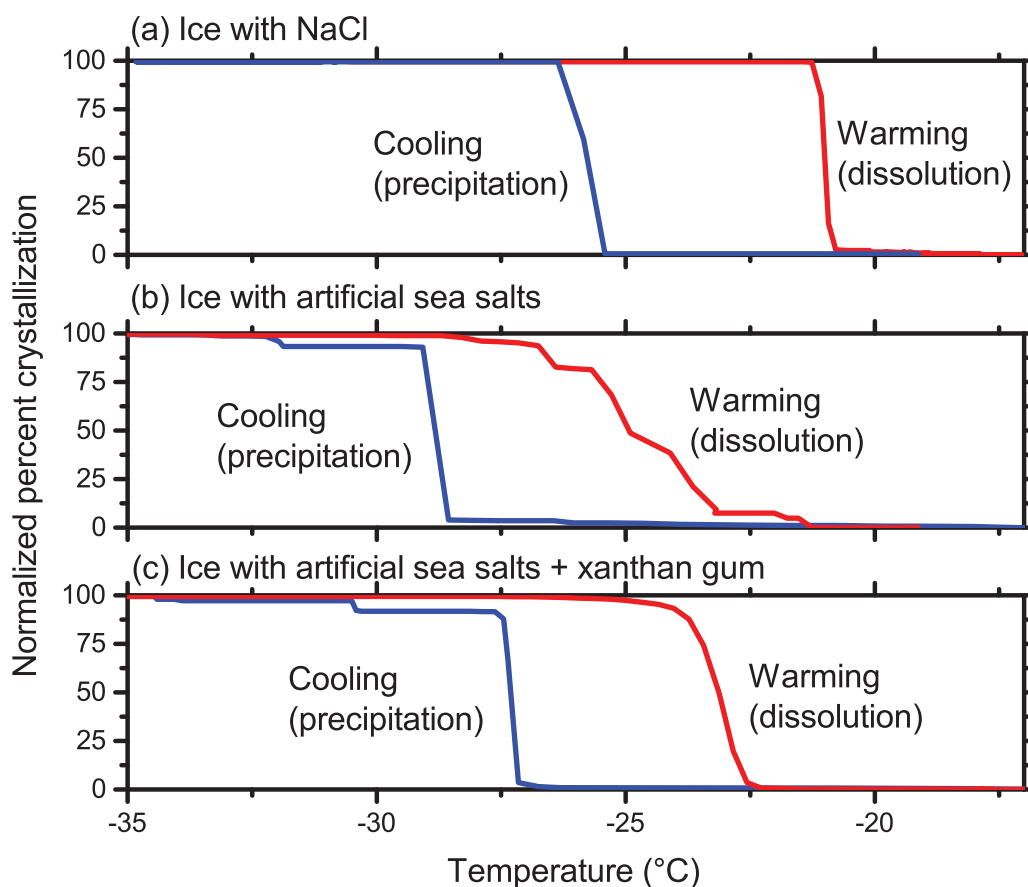


**Figure 9.** Selected experimental runs showing hysteresis of hydrohalite precipitation and dissolution during temperature cycling in three sections from different types of artificial sea ice. In all cases, the brine inclusions do not crystallize until well below the expected precipitation temperature of  $-21.1^{\circ}\text{C}$  for NaCl and  $-22.9^{\circ}\text{C}$  for sea salt.

than inhibit it, perhaps by nucleating hydrohalite crystals. Extracellular polysaccharides can differ in their chemical properties, so it is possible that EPS made by microbes native to sea ice could be adapted specifically to interact with hydrohalite, whereas xanthan gum (which is made by a soil microbe) would be less likely to have such an adaptation.

Each graph in Figures 8 and 9 represents analysis of a representative  $30\text{ mm}^2$  area of a single section, so these results should be considered somewhat qualitative. Given the uneven nature of sea ice structure at the scale being considered, and the unpredictable pattern of brine pocket crystallization, each repetition of the experiment was expected to give slightly different results. Determining the exact effect of brine-pocket size and shape on the timing of hydrohalite precipitation would require many more experimental runs and more complex image analysis. Such an experiment could be a promising candidate for future study.

### 3.3. Effects of Freezing Rate and Brine Volume

An additional experiment was carried out to investigate the effects of the rate of change in temperature. A sample containing artificial sea salts and xanthan gum was placed in the cold room using the same setup as before, but this time the temperature was lowered in  $2^{\circ}$  steps and allowed to remain steady for approximately 48 h at each step. We expected that the hydrohalite precipitation might occur at a higher temperature when given time to equilibrate. Contrary to our expectations, we found that the precipitation pattern of the hydrohalite within brine inclusions in this ice section was substantially similar to that of more rapidly cooled sections. The first precipitation occurred around  $-26^{\circ}\text{C}$ , and small brine inclusions continued to precipitate even at  $-35^{\circ}\text{C}$  and below, after spending more than 10 days below  $-23^{\circ}\text{C}$ .

As described in section 3.1, we noted that precipitation in any individual brine pocket was always rapid and complete; the brine pocket would be filled with hydrohalite crystals within one time step (5–15 min) and

**Table 1.** Temperature at Which Salt and Ice Precipitated in 40 mL Beakers<sup>a</sup>

Solution	Precipitation Temperature (°C)
233‰ NaCl (this work)	−22.6
226‰ NaCl [Toner <i>et al.</i> , 2014]	−27.9
260‰ NaCl [Toner <i>et al.</i> , 2014]	−29.6
233‰ artificial sea salt (this work)	−24.2
233‰ artificial sea salt + 1‰ xanthan gum (this work)	−24

<sup>a</sup>These volumes of solution, larger than brine inclusions by a factor of  $\sim 10^7$ , show very little supersaturation, precipitating at most 1.5 K below the expected temperature. The samples were cooled further to  $-30^\circ\text{C}$  with no significant additional precipitation.

change very little afterward. This observation suggests that precipitation within supersaturated brine is initiated by the chance formation of a single crystal and then propagates rapidly through the whole pocket. In this case, a larger volume of brine should show less supersaturation, since it would be more likely to contain a crystallization nucleus. If larger volumes of brine promote crystallization, this phenomenon would represent another mechanism by which the presence of EPS could enhance crystallization in some cases, as EPS is known to increase the interconnectivity (and therefore the effective size) of brine inclusions [Krembs *et al.*, 2011].

To test this idea, we put solutions of brine at 233‰ salinity, similar to what would be found in the brine

inclusions near the precipitation temperature, into 40 mL polyethylene bottles and placed them in a cold room at  $-37^\circ\text{C}$ . In this experiment, we used a temperature probe (inserted through a hole in the top of the bottle) to detect crystallization, by observing the rate of cooling over time and identifying plateaus where phase transitions were taking place. The solutions were of the same types as the ones used in creating artificial sea ice (NaCl, sea salts, and sea salts with 1000 mg/L xanthan gum). In these containers, with a volume about  $10^7$  times the size of a brine pocket, no supersaturation occurred; precipitation took place near the nominal precipitation temperature of the solutions (Table 1). However, similar experiments conducted by Toner *et al.* [2014] found significant supersaturation. In those experiments, the supersaturation persisted even when the salt solution was mixed with soil to provide nucleation points for hydrohalite.

## 4. Discussion

### 4.1. Fieldwork

The fieldwork results show small systematic increases in albedo with decreasing temperatures. Interpretation of these data is complicated by the fact that these measurements at different temperatures were also made on different days. Most notably, blowing snow could stick to the ice and increase its albedo; this possibility was strikingly demonstrated by the reformation of the snow crust several days after it was originally removed. Frost might also have formed on the surface. We did visually inspect the ice before each measurement, and brushed away any apparent deposits of snow. It is conceivable, however, that frost or blown snow could have accumulated enough to influence the measurements without being visually apparent. Over the period during which we regularly visited the study site, however, the general trend was toward thinning or disappearance of snow crusts. In many areas, the snow crust, which had appeared optically thick when first observed, became thin and patchy over the subsequent weeks.

The spectral albedos in Figure 5 show a nearly constant increase in albedo across the measured wavelengths for the three measurements made when the ice was below the expected precipitation temperature for hydrohalite. All of the measurements show a slight peak around 500 nm. The decrease in albedo with decreasing wavelength from 500 to 350 nm suggests contamination by absorbing particles, since ice and water are essentially nonabsorptive in this wavelength region but mineral dust contains iron oxides whose absorption increases with decreasing wavelength. The wind that blew fallen snow away from (and sometimes onto) the ice at this location also transported volcanic dust from Tent Island, so the ice surface contained some dust which would have lowered the albedo at visible and UV wavelengths [Warren and Wiscombe, 1980, Figure 5; Warren, 1982, Figure 7]. The crossover of the albedo curves for 5 October and 22 September in Figure 5 could occur if the ice measured on 22 September contained more dust. The influence of the dust would be greatest at  $\lambda < 500$  nm, whereas absorption by ice and water becomes significant at longer wavelengths, resulting in a peak at  $\lambda \approx 500$  nm (see Warren *et al.* [2006, Figure 2] and the associated discussion.)

During all measurements, the ice was warmer at a depth of 10 cm than at the surface. This temperature gradient almost certainly led to a gradient in the amount of hydrohalite precipitation, with more precipitation, and therefore more scattering of light, occurring in the uppermost colder ice.

#### 4.2. Laboratory Work

Our technique for measuring the amount of hydrohalite precipitation relies on analyzing two-dimensional images of thin sections photographed in transmitted light. This technique has some limitations that compromise its accuracy. It captures only the cross-sectional area of the brine inclusion, not its volume, so it does not necessarily represent the total amount of hydrohalite in the brine inclusions. In order to quantitatively determine the amount of brightening expected based on a given amount of hydrohalite precipitation, we would need to know the volume and number of brine inclusions that had crystallized. The shape of the inclusions would also influence the albedo of the ice. Determining brine pocket shape and volume from two-dimensional images, however, is nonunique, and it would be necessary to analyze a large population of brine inclusions to understand the distribution of shape and size. Moreover, our cold room was evidently unable to achieve a sufficiently low temperature to cause all brine inclusions to precipitate. Some brine pockets in the thin sections we imaged did not show hydrohalite crystallization, perhaps because the temperature was not low enough. Because of these limitations, we draw no quantitative conclusions from these precipitation experiments. They simply demonstrate qualitatively that precipitation can occur gradually over time, and that it exhibits hysteresis.

In some ways, the results of our laboratory experiments complicate the interpretation of the field albedos, since field albedos show an increase even at  $-23^{\circ}\text{C}$ , whereas brine inclusions in the laboratory did not precipitate until  $-26^{\circ}\text{C}$  or below. However, the laboratory experiments were necessarily conducted on just a few brine inclusions, whose size was somewhat limited by the experimental technique itself, since large brine inclusions would intersect the surface of the thin ice section and drain, or even cause the section to break during microtoming and be discarded. Among the hundreds of millions of brine inclusions near the surface of a square meter of natural sea ice [Light *et al.*, 2003], it seems likely that some possess the right properties—perhaps large size or the presence of material that can act as a nucleation site—to precipitate at  $-23^{\circ}\text{C}$ . Future work could include radiative transfer modeling to show what percentage of pockets would need to precipitate to account for the observed increase in albedo, along with more laboratory analysis of what properties of a brine pocket influence its precipitation.

#### 4.3. Implications for Snowball Earth

As temperature decreases, the precipitation of salt within brine inclusions causes the albedo to rise, leading to further cooling and thus a positive feedback on the progression to a frozen ocean. This bare subeutectic sea ice would be the surface type on the ocean in snow-free regions; i.e., regions of net sublimation.

The effect of hydrohalite precipitation on the climate of Snowball Earth would be enhanced by an additional positive feedback. As sublimation continues during the cold early part of a snowball event, precipitated hydrohalite is expected to accumulate on the surface of the ice as a lag deposit. In laboratory experiments this lag deposit, with its small crystals of hydrohalite, forms a brightly reflective white surface [Light *et al.*, 2009, Figure 5c].

#### Acknowledgments

This research was supported by NSF grants ANT-07-39779 and ANT-11-42963. We thank the staff of McMurdo Station for their assistance in supporting our field campaign. We also thank Andrew Mahoney and Alex Gough (New Zealand Antarctic Programme) for their winter observations of McMurdo sea ice and assistance with preparing thin sections using their microtome at Scott Base. We acknowledge Hajo Eicken and Bonnie Light for helpful discussion. Helpful comments on the manuscript were provided by Jody Deming, Bonnie Light, and two anonymous reviewers. The data used to generate the figures in this paper may be found at <http://dx.doi.org/10.6084/m9.figshare.1258839>.

#### References

- Abbot, D. S., A. Voigt, and D. Koll (2011), The Jormungand global climate state and implications for Neoproterozoic glaciations, *J. Geophys. Res.*, *116*, D18103, doi:10.1029/2011JD015927.
- Abràmoff, M. D., P. J. Magalhães, and S. J. Ram (2004), Image processing with Image, *J. Biophotonics Int.*, *11*(7), 36–43.
- Brandt, R. E., and S. G. Warren (1993), Solar heating rates and temperature profiles in Antarctic snow and ice, *J. Glaciol.*, *39*, 99–110.
- Brandt, R. E., S. G. Warren, A. P. Worby, and T. C. Grenfell (2005), Surface albedo of the Antarctic sea-ice zone, *J. Clim.*, *18*, 3606–3622.
- Cox, G. F. N., and W. F. Weeks (1988), Numerical simulations of the profile properties of undeformed first-year sea ice during the growth season, *J. Geophys. Res.*, *93*, 12,449–12,460.
- Dadic, R., P. C. Mullen, M. Schneebeli, R. E. Brandt, and S. G. Warren (2013), Effects of bubbles, cracks, and volcanic tephra on the spectral albedo of bare ice near the Trans-Antarctic Mountains: Implications for sea-glaciers on Snowball Earth, *J. Geophys. Res. Earth Surf.*, *118*, 1658–1676, doi:10.1002/jgrf.20098.
- Goodman, J. C. (2006), Through thick and thin: Marine and meteoric ice in a “Snowball Earth” climate, *Geophys. Res. Lett.*, *33*, L16701, doi:10.1029/2006GL026840.
- Goodman, J. C., and R. T. Pierrehumbert (2003), Glacial flow of floating marine ice in Snowball Earth, *J. Geophys. Res.*, *108*(C10), 3308, doi:10.1029/2002JC001471.
- Han, B., and J. C. Bischof (2004), Direct cell injury associated with eutectic crystallization during freezing, *Cryobiology*, *48*, 8–21.
- Hoffman, P. F., and D. P. Schrag (2002), The snowball Earth hypothesis: Testing the limits of global change, *Terra Nova*, *14*(3), 129–155.
- Hu, Y.-B., D. A. Wolf-Gladrow, G. S. Dieckmann, C. Völker, and G. Nehrke (2014), A laboratory study of ikaite ( $\text{CaCO}_3 \cdot 6\text{H}_2\text{O}$ ) precipitation as a function of pH, salinity, temperature and phosphate concentration, *Mar. Chem.*, *162*, 10–18.
- Kindel, B. C., Z. Qu, and A. F. H. Goetz (2001), Direct solar spectral irradiance and transmittance measurements from 350 to 2500 nm, *Appl. Opt.*, *40*, 3483–3494, doi:10.1364/AO.40.003483.

- Krembs, C., H. Eicken, K. Junge, and J. W. Deming (2002), High concentrations of exopolymeric substances in Arctic winter sea ice: Implications for the polar ocean carbon cycle and cryoprotection of diatoms, *Deep Sea Res., Part I*, 49(12), 2163–2181.
- Krembs, C., H. Eicken, and J. W. Deming (2011), Exopolymer alteration of physical properties of sea ice and implications for ice habitability and biogeochemistry in a warmer Arctic, *Proc. Natl. Acad. Sci. U. S. A.*, 108(9), 3653–3658.
- Light, B., G. A. Maykut, and T. C. Grenfell (2003), Effects of temperature on the microstructure of first-year Arctic sea ice, *J. Geophys. Res.*, 108(C2), 3051, doi:10.1029/2001JC000887.
- Light, B., G. A. Maykut, and T. C. Grenfell (2004), A temperature-dependent, structural-optical model of first-year sea ice, *J. Geophys. Res.*, 109, C06013, doi:10.1029/2003JC002164.
- Light, B., R. E. Brandt, and S. G. Warren (2009), Hydrohalite in cold sea ice: Laboratory observations of single crystals, surface accumulations, and migration rates under a temperature gradient, with application to “Snowball Earth”, *J. Geophys. Res.*, 114, C07018, doi:10.1029/2008JC005211.
- Light, B., R. C. Carns, and S. G. Warren (2015), “Albedo dome”: A method for measuring spectral flux-reflectance in a laboratory for media with long optical paths, *Appl. Opt.*, 54(17), 5260–5269, doi:10.1364/AO.54.005260.
- Marion, G. M., R. E. Farren, and A. J. Komrowski (1999), Alternative pathways for seawater freezing, *Cold Reg. Sci. Technol.*, 29(3), 259–266.
- McClatchey, R. A., R. W. Fenn, J. E. A. Selby, F. E. Volz, and J. S. Garing (1972), *Optical Properties of the Atmosphere*, 3rd ed., Rep. AFCRL-72-0497, 108 pp., Air Force Cambridge Res. Lab., Hanscom Air Force Base, Bedford, Mass.
- Perovich, D. K. (1979), The optical properties of young sea ice, MS thesis, Univ. of Wash., Seattle, Wash.
- Perovich, D. K., and A. J. Gow (1991), A statistical description of the microstructure of young sea ice, *J. Geophys. Res.*, 96, 16,943–16,953.
- Perovich, D. K., and A. J. Gow (1996), A quantitative description of sea ice inclusions, *J. Geophys. Res.*, 101, 18,327–18,343.
- Perovich, D. K., and T. C. Grenfell (1981), Laboratory studies of the optical properties of young sea ice, *J. Glaciol.*, 27(96), 331–346.
- Perovich, D. K., and J. A. Richter-Menge (1994), Surface characteristics of lead ice, *J. Geophys. Res.*, 99, 16,341–16,350.
- Pierrehumbert, R. T. (2005), Climate dynamics of a hard snowball Earth, *J. Geophys. Res.*, 110, D01111, doi:10.1029/2004JD005162.
- Pierrehumbert, R. T., D. S. Abbot, A. Voigt, and D. Koll (2011), Climate of the Neoproterozoic, *Annu. Rev. Earth Planet. Sci.*, 39, 417–460.
- Pollard, D., and J. F. Kasting (2004), Climate-ice sheet simulations of Neoproterozoic glaciation before and after collapse to Snowball Earth, in *The Extreme Proterozoic: Geology, Geochemistry, and Climate*, *Geophys. Monogr. Ser.*, vol. 146, edited by G. Jenkins et al., pp. 91–105, AGU, Washington, D. C.
- Pollard, D., and J. F. Kasting (2005), Snowball Earth: A thin-ice solution with flowing sea glaciers, *J. Geophys. Res.*, 110, C07010, doi:10.1029/2004JC002525.
- Pollard, D., and J. F. Kasting (2006), Reply to comment by Stephen G. Warren and Richard E. Brandt on “Snowball Earth: A thin-ice solution with flowing sea glaciers”, *J. Geophys. Res.*, 111, C09017, doi:10.1029/2006JC003488.
- Pringle, D., G. Dubuis, and H. Eicken (2009), Impedance measurements of the complex dielectric permittivity of sea ice at 50 MHz: Pore microstructure and potential for salinity monitoring, *J. Glaciol.*, 55, 81–94.
- Purdie, C., P. Langhorne, G. Leonard, and T. Haskell (2006), Growth of first year land-fast Antarctic sea ice determined from winter temperature measurements, *Ann. Glaciol.*, 44, 170–176.
- Rankin, A. M., E. M. Wolff, and S. Martin (2002), Frost flowers: Implications for tropospheric chemistry and ice core interpretation, *J. Geophys. Res.*, 107(D23), 4683, doi:10.1029/2002JD002492.
- Spencer, R. J., N. Möller, and J. H. Weare (1990), The prediction of mineral solubilities in natural waters: A chemical equilibrium model for the Na-K-Ca-Mg-Cl-SO<sub>4</sub>-H<sub>2</sub>O system at temperatures below 25 C, *Geochim. Cosmochim. Acta*, 54, 575–590.
- Style, R. W., and M. G. Worster (2009), Frost flowers on sea ice and lake ice, *Geophys. Res. Lett.*, 36, L11501, doi:10.1029/2009GL037304.
- Toner, J. D., D. C. Catling, and B. Light (2014), The formation of supercooled brines, viscous liquids, and low-temperature perchlorate glasses in aqueous solutions relevant to Mars, *Icarus*, 233, 36–47, doi:10.1016/j.icarus.2014.01.018.
- Untersteiner, N. (1968), Natural desalination and equilibrium salinity profile of perennial sea ice, *J. Geophys. Res.*, 73, 1251–1257.
- Warren, S. G. (1982), Optical properties of snow, *Rev. Geophys.*, 20, 67–89.
- Warren, S. G., and R. E. Brandt (2006), Comment on “Snowball Earth: A thin-ice solution with flowing sea glaciers” by David Pollard and James F. Kasting, *J. Geophys. Res.*, 111, C09016, doi:10.1029/2005JC003411.
- Warren, S. G., and W. J. Wiscombe, (1980), A model for the spectral albedo of snow, II: Snow containing atmospheric aerosols, *J. Atmos. Sci.*, 37, 2734–2745.
- Warren, S. G., R. E. Brandt, T. C. Grenfell, and C. P. McKay (2002), Snowball Earth: Ice thickness on the tropical ocean, *J. Geophys. Res.*, 107(C10), 3167, doi:10.1029/2001JC001123.
- Warren, S. G., R. E. Brandt, and T. C. Grenfell (2006), Visible and near-ultraviolet absorption spectrum of ice from transmission of solar radiation into snow, *Appl. Opt.*, 45(21), 5320–5334, doi:10.1364/AO.45.005320.
- Weeks, W. F., and S. F. Ackley (1982), The growth, structure and properties of sea ice, in *Sea Ice, CRREL Monogr.*, vol. 82–1, Cold Reg. Res. Eng. Lab., Hanover, N. H.
- Wettlaufer, J. S. (1998), Introduction to crystallization phenomena in natural and artificial sea ice, in *Physics of Ice-covered Seas*, edited by M. Leppäranta, pp. 105–194, Univ. of Helsinki Press, Helsinki, Finland.
- Wiscombe, W. J., R. M. Welch, and W. D. Hall (1984), The effects of very large drops on cloud absorption, Part I, Parcel models, *J. Atmos. Sci.*, 41, 1336–1355.
- Yang, J., W. R. Peltier, and Y. Hu (2012), The initiation of modern “Soft Snowball” and “Hard Snowball” climates in CCSM3, Part I: The influences of solar luminosity, CO<sub>2</sub> concentration, and the sea ice/snow albedo parameterization, *J. Clim.*, 25, 2711–2736, doi:10.1175/JCLI-D-11-00189.